Stanford Exploration Project, Report 75, November 17, 1997, pages 41–52

Migration velocity dependence of plumes

James L. Black, Dimitri Bevc, and Gopal Palacharla[1]

keywords: *velocity, time migration, diffraction*

ABSTRACT

Changing the migration velocity causes the response of time migration to a point diffractor beneath a lateral velocity variation to evolve. At the extremes of migration velocity, the image is either fully undermigrated or fully overmigrated. Between these extremes, there is the mixture of overmigration and undermigration that leads to "plume" responses. As the velocity is changed, these plumes transform and rotate in a systematic manner. A simple first-order theory of plume velocity dependence explains some, but not all, of the observed behavior.

INTRODUCTION

In practice, it is usually difficult to choose the correct velocity for migration. For depth migration, it is generally accepted that the best choice is the velocity that optimally focuses the image. But what happens when we use time migration to focus the image? We often employ time migration to image events when there are lateral velocity variations present. In these situations, it is generally impossible to completely focus the image even when the correct velocity is used. For example, in Black *et. al.* (1992) we showed that time migration with the *correct* migration velocity collapses a point diffractor not to a point but to a cusp-shaped curve that we called a "plume". It is therefore interesting to study the effect of migration velocity on the plume response in a `v(x)` medium, and that is the purpose of this paper. Here we use both a geometrical construction and actual migrations of synthetic data to demonstrate the diffractor response of time migration in such a medium. The plume response described in Black *et. al.* (1992) is shown to rotate and change shape with changing migration velocity. We gain some insight into this behavior by developing a simple first-order theory of plume rotation analogous to Black and Brzostowski (1993).

Since we will be building on the material presented in Black *et. al.* (1992), we will refer to that paper as Paper 1.

[1]**email:** not available

VARIATION OF MIGRATION VELOCITY

Synthetic Model

The model used in this paper is the same as that used in Paper 1 (Figure 1). An implicit velocity gradient is caused by the dipping-layer since the velocity changes across it. The plume response due to a point diffractor positioned at a depth of 4 kft at a horizontal position of 8 kft is displayed in Figure 2. This is the Kirchhoff modeling and migration result discussed in Paper 1. The migration velocity is the vertical RMS well velocity of 8.84 kft/s that would be obtained along a well drilled straight down into the diffractor from the surface. The first-order theory derived by Black and Brzostowski (1993) and reviewed in Paper 1 predicts that the plume shape is given by:

$$x_k \approx x_m + A(x_m, z_m)(1 + 3\tan^2\theta) \tag{1}$$

$$\frac{v_2 t_k}{2} \approx \frac{v_2 t_m}{2} - 2A(x_m, z_m)\tan^3\theta \tag{2}$$

where x_k and t_k are the spatial and temporal coordinates of the time migrated points and θ is the propagation angle. This is the symmetric curve overlaid on the migration result of Figure 2. As discussed in Paper 1, this theoretical curve accounts for some of the features of the plume but lacks the higher-order terms which account for plume asymmetry.

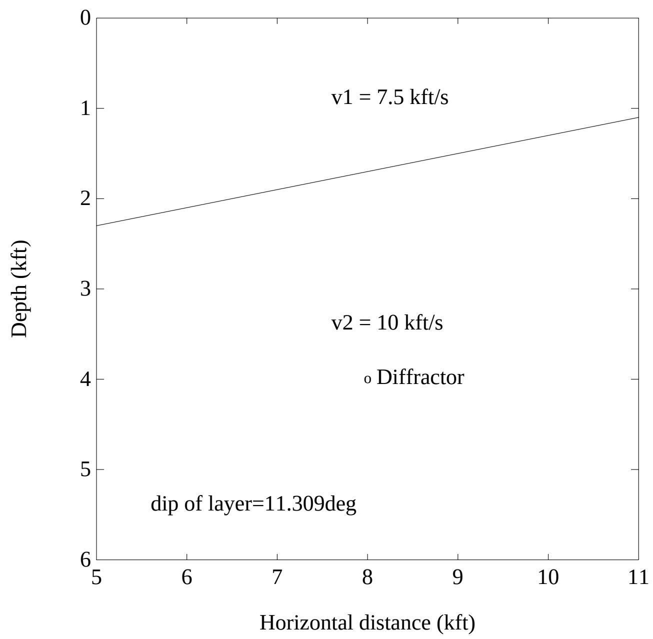

Figure 1: Dipping-layer model. The change in velocity across the dipping layer causes an implicit velocity gradient which depends on the dip of the layer. dimitri2-gem1 [NR]

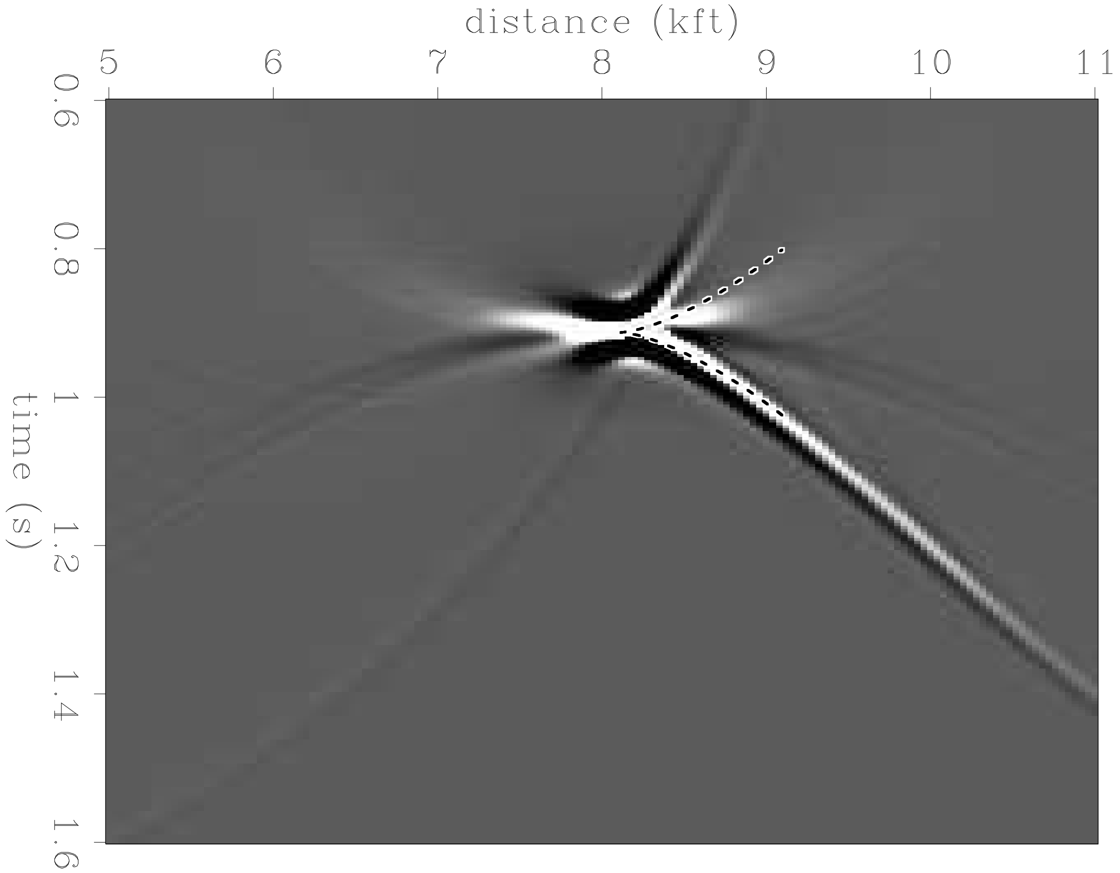

Figure 2: Comparison of the analytic expression for the plume to the Kirchhoff migration result. dimitri2-analytic [ER]

Observed Effect of Migration Velocity Changes

In practice, it is difficult to choose the correct velocity for migration. It is therefore instructive to see what effect the variation of migration velocity has in a `v(x)` medium. The synthetic data from Paper 1 are migrated with a Kirchhoff algorithm using various migration velocities and displayed in Figure 3. Each frame is migrated using a different constant velocity. The velocities used are 7.5 kft/s to 11.5 kft/s in increments of 0.5 kft/s. The image changes from undermigrated in the upper left corner to overmigrated in the lower right corner. The fourth frame (`Vmig=9.0`) is migrated with a velocity close to the RMS well velocity (8.84 kft/s) used in Figure 2.

As migration velocity is increased the image begins to develop an upper limb in the third frame (`Vmig=8.5`) of Figure 3. The plume is well formed in the fourth frame (`Vmig=9.0`) and then appears to rotate clockwise as migration velocity is increased. In the last frame the lower limb of the plume is very faint and the image looks overmigrated.

By scrutinizing the frames of the movie in Figure 3, we can see how the plume is formed. The left limb of the undermigrated image in frame 1 (`Vmig=7.5`) gets swept upward and becomes the upper limb of the plume in frame 4 (`Vmig=9.0`). Recall that the low velocity wedge (Figure 1) has the effect of making the left side of the true diffraction curve overmigrated and the right side undermigrated when the RMS well velocity is used. This overmigration sweeps the limb upwards. The right limb of the undermigrated image in frame 1 (`Vmig=7.5`) remains undermigrated as velocity increases until the last few frames where the typical overmigration "smile" begins to form.

The nature of plume variation with migration velocity is examined for a different range of migration velocity with smaller increments of migration velocity variation around the RMS well velocity in Figure 4. The center frame ($\triangle V_{mig}$ =0.0) is migrated with the RMS well velocity of 8.84 kft/s. The image in the first two frames is a characteristic undermigration "frown" and the image in the last frame is a characteristic overmigration "smile". As in Figure 3, we can see the left side of the diffraction curve being swept up to form the upper limb of the plume while the right side of the diffraction curve eventually forms the left side of the "smile". Migration velocities close to the RMS well velocity frames 3 ($\triangle V_{mig}$ =-0.2) through 7 ($\triangle V_{mig}$ =0.2) show the plume rotating slightly clockwise, although the overall rotation trend evident in frames 2 through 8 is somewhat counterclockwise.

AGREEMENT WITH GEOMETRICAL CONSTRUCTION

The tangent construction method described in Paper 1 is used to study the kinematics of the plume as a function of migration velocity. The tangent construction result presented in Figure 5 uses the same velocities used in Figure 4. The image begins as an undermigrated "frown", becomes a clockwise rotating plume in frames 3 ($\triangle V_{mig}$ =-

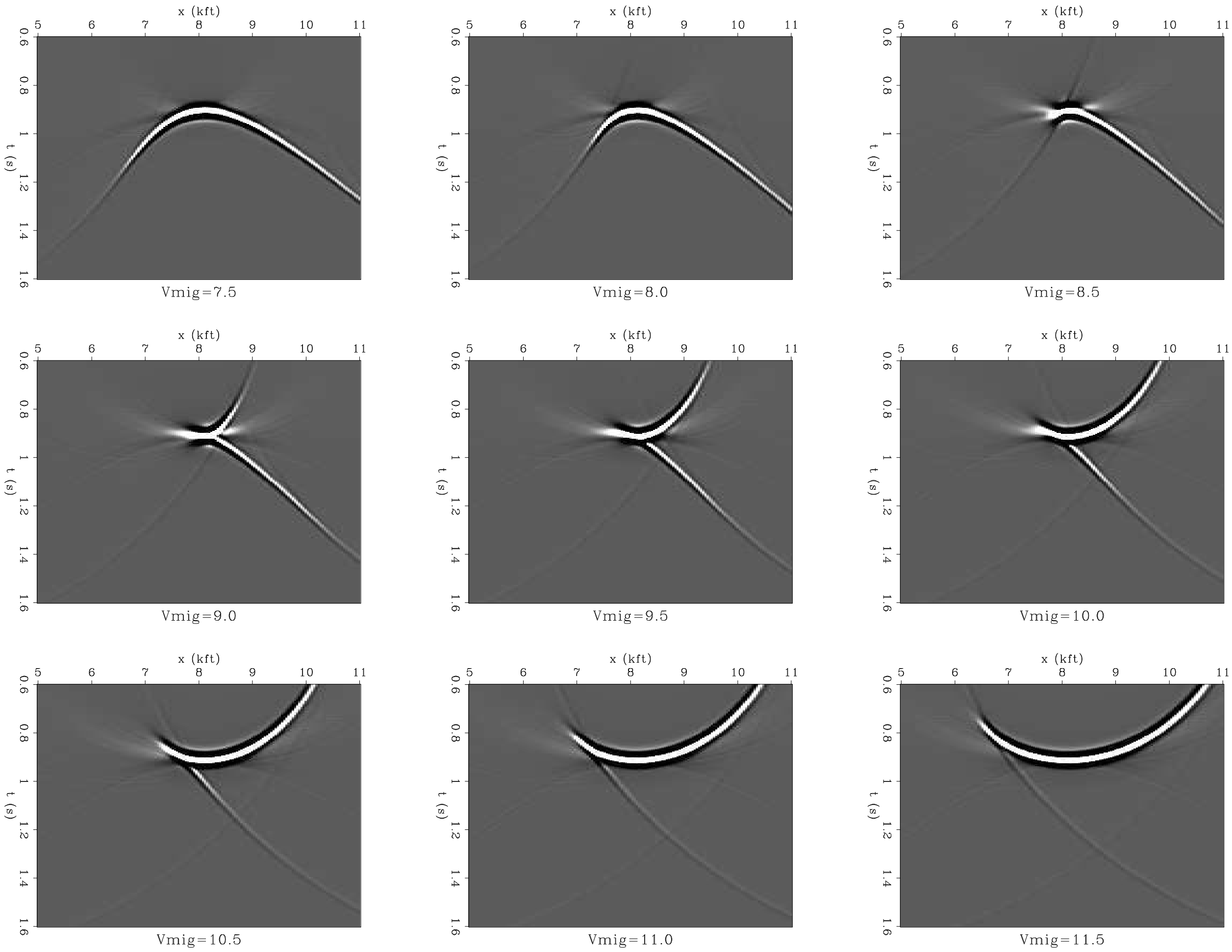

Figure 3: Kirchhoff migration with a range of velocities. The constant migration velocity ranges from 7.5 kft/s to 11.5 kft/s. The RMS well velocity at the diffractor position is 8.84 kft/s. If you have the electronic version of this report you can click on the button and see a movie of the image as a function of migration velocity. The movie begins with the *true-diffraction curve* as the first frame and then sweeps through the images for migration velocities ranging from 6.0 kft/s to 12.5 kft/s in steps of 0.5 kft/s. $\boxed{\text{dimitri2-movie}}$ [ER]

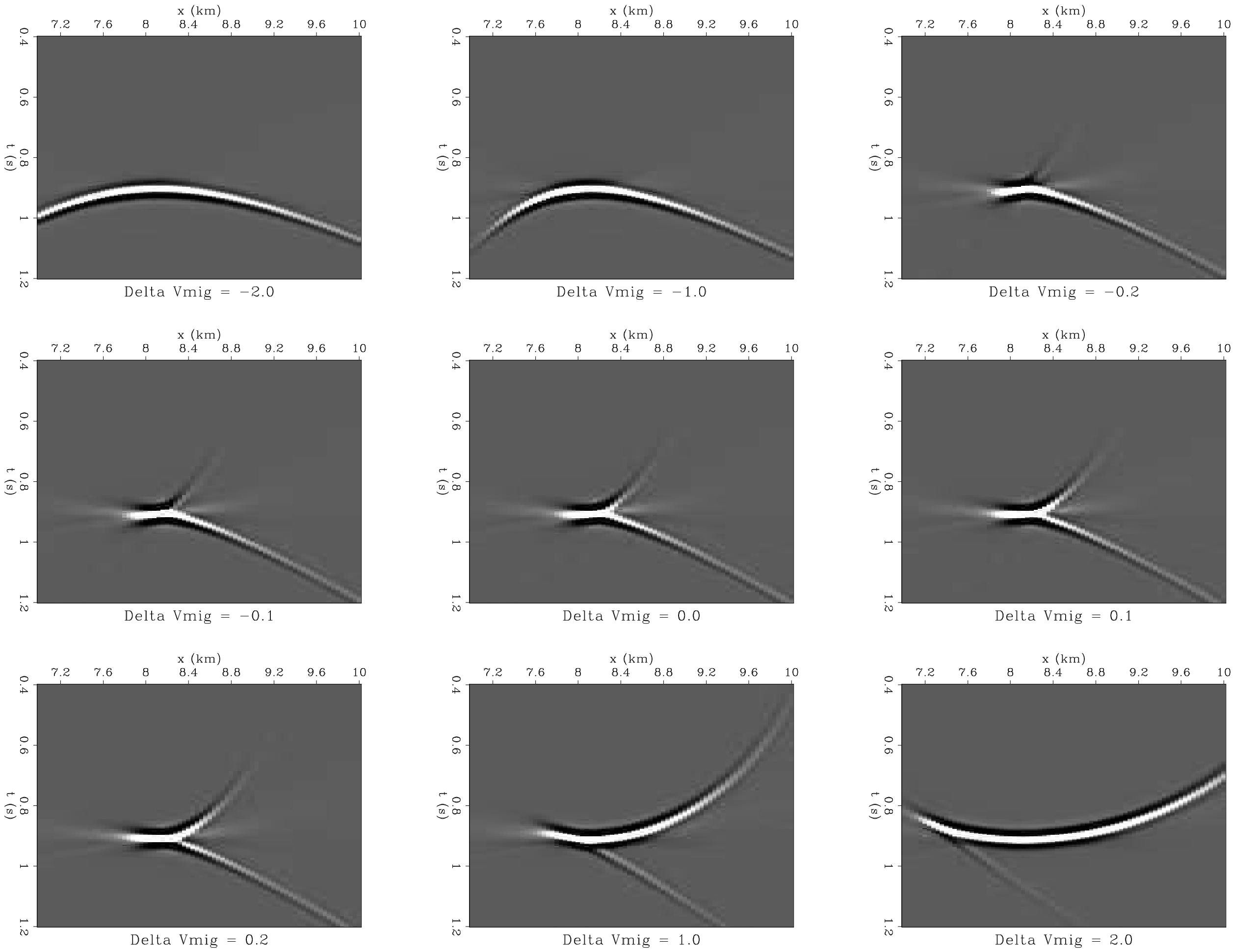

Figure 4: Kirchhoff migration with various migration velocities. The center frame is migrated with the RMS well velocity of 8.84 kft/s. The other frames are migrated with velocities of $V_{mig} = V_{rmswell} + \triangle V_{mig}$. The $\triangle V_{mig}$ values are given under the frame in units of kft/s. $\boxed{\text{dimitri2-kfrot}}$ [ER]

0.2) through 7 ($\triangle V_{mig}$ =0.2), and finally forms the overmigration "smile". It is once again evident that the left side of the diffraction curve becomes the upper limb of the plume and the right side of the diffraction curve eventually becomes the left side of the "smile". Note the very close agreement between Figure 5 and Figure 4.

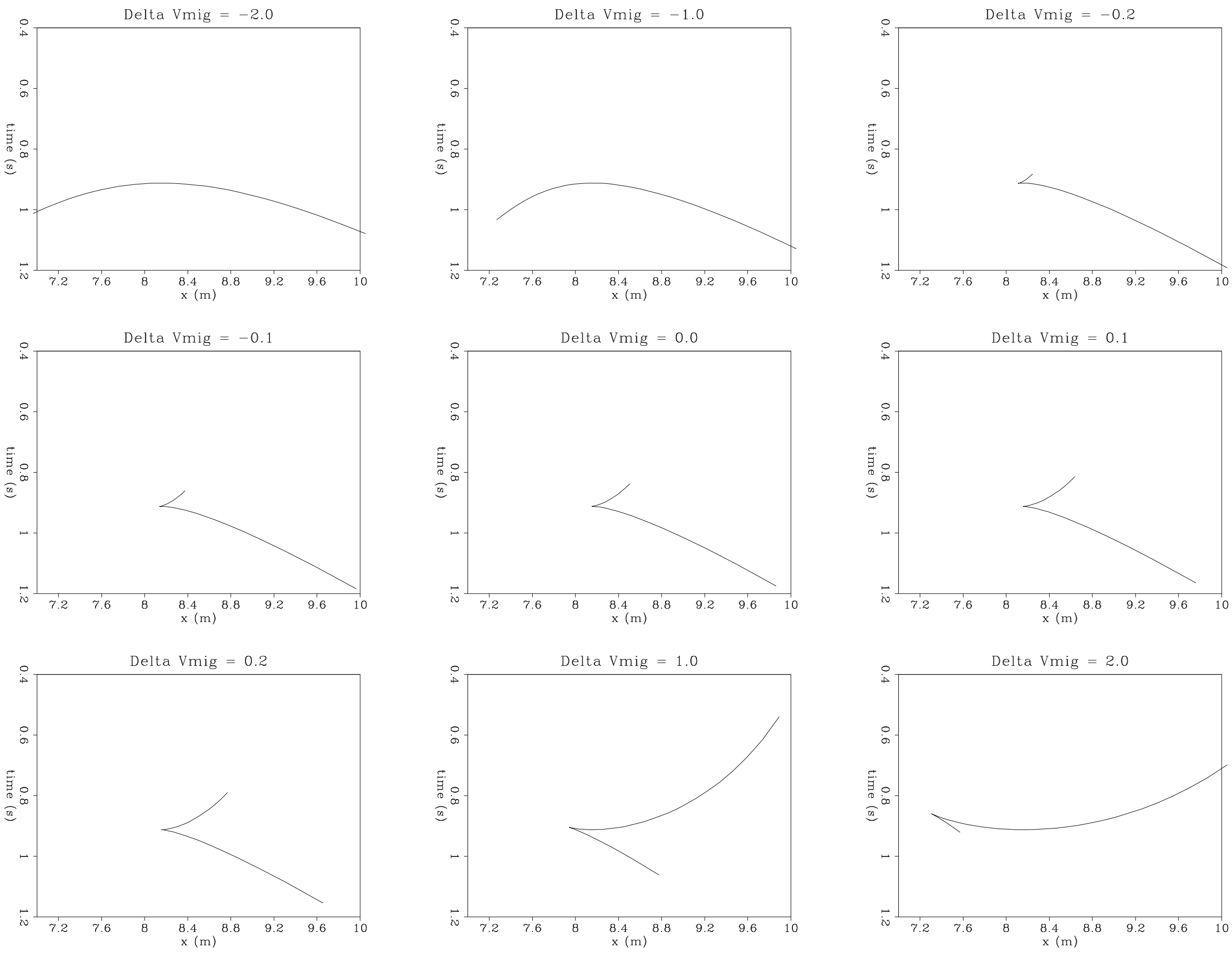

Figure 5: Tangent construction. The same migration velocities used in Figure 4 are used here. dimitri2-vels [ER]

FIRST-ORDER THEORY OF PLUME VELOCITY DEPENDENCE

The first-order theory of plume velocity dependence is developed here following steps similar to Black and Brzostowski (1993) and Paper 1.

We begin with the zero-offset *time migration curve*:

$$t_0^2 = t_k^2 + 4\left[\frac{x_0 - x_k}{V_{mig}}\right]^2 \tag{3}$$

Defining the velocity contrast across the dipping reflector in Figure 6 as

$$\gamma = \frac{v_2 - v_1}{v_2},$$

and the dip angle as θ_1, Black and Brzostowski (1993) use the geometry of Figure 6 to express the *true diffraction curve* to first order in γ and $\sin\theta_1$ as:

$$x_0 - x_m \approx -z_m \tan\theta + \gamma d_1 \frac{\sin\theta}{\cos^3\theta} - \gamma \sin\theta_1 z_m \frac{1}{\cos^4\theta} + A\frac{1+\sin^2\theta}{\cos^4\theta} \tag{4}$$

$$\frac{v_2 t_0}{2} \approx \frac{z_m}{\cos\theta} + \gamma d_1 \frac{1 - 2\sin^2\theta}{\cos^3\theta} + \gamma\sin\theta_1 z_m \frac{\sin\theta}{\cos^4\theta} - 2A\frac{\sin^3\theta}{\cos^4\theta}, \tag{5}$$

where the quantity A is defined as

$$A(x_m, z_m) = d_2 \gamma \sin\theta_1. \tag{6}$$

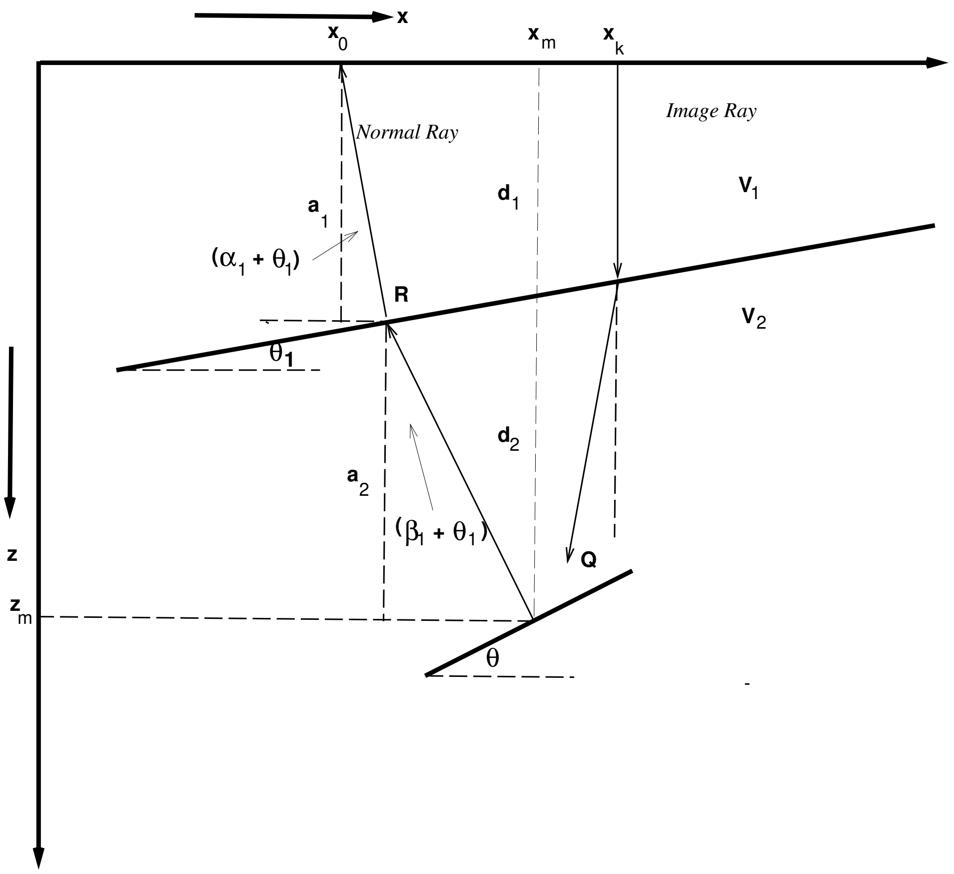

Figure 6: Geometry and raypaths for the dipping layer model. The diffractor is positioned at (x_m, z_m). The spatial and temporal coordinates of the diffraction curve and time migrated image are given by (x_0, z_0) and (x_k, z_k), respectively. dimitri2-fig2 [NR]

Matching the slope of the *time migration curve* with the time dip D of the *true diffraction curve* leads to the following formulas for the position of the time migrated point (x_k, t_k):

$$x_k = x_0 - \left[\frac{V_{mig}D}{2}\right]\left[\frac{V_{mig}t_0}{2}\right], \tag{7}$$

$$t_k = t_0\sqrt{1 - \left[\frac{V_{mig}D}{2}\right]^2}, \tag{8}$$

where the time dip D can be expressed to first order in γ and $\sin\theta_1$ as:

$$\frac{v_2 D}{2} \approx -\sin\theta - \gamma\frac{\sin\theta_1}{\cos\theta}. \tag{9}$$

Black and Brzostowski (1993) define the RMS migration velocity $V(x_m, t_m)$ at the correct migrated position (x_m, t_m) to first-order in γ and $\sin\theta_1$ as:

$$\left[\frac{V(x_m, t_m)}{v_2}\right]^2 \approx 1 - 2\gamma\frac{d_1}{z_m}. \tag{10}$$

Since we are interested in the variation of the plume operator with migration velocity, we define

$$V_{mig} = V(x_m, t_m) + \triangle V_{mig} = V(x_m, t_m)\left(1 + \frac{\triangle V_{mig}}{V(x_m, t_m)}\right). \tag{11}$$

Considering small values of $\triangle V_{mig}$ so that

$$\frac{\triangle V_{mig}}{V(x_m, t_m)} \leq \gamma,$$

we can expand V_{mig}^2 retaining only first-order terms as:

$$V_{mig}^2 \approx V(x_m, t_m)^2\left(1 + 2\frac{\triangle V_{mig}}{V(x_m, t_m)}\right). \tag{12}$$

We are finally ready to derive the first-order theory of plume velocity dependence.

Time migration is carried out by inserting equations (4), (5), (10), and (12) into equations (7) and (8). Retaining only the terms which are first order in γ and $\sin\theta_1$ allows us to express the first order theory for a perturbation in migration velocity by the following equations:

$$x_k = x_m + A(1 + 3\tan^2\theta) + \frac{2\triangle V_{mig}}{V_{mig}} z_m \tan\theta \tag{13}$$

$$\frac{v_2 t_k}{2} = \frac{v_2 t_m}{2} - 2A\tan^3\theta - \frac{\triangle V_{mig}}{V_{mig}} z_m \tan^2\theta \tag{14}$$

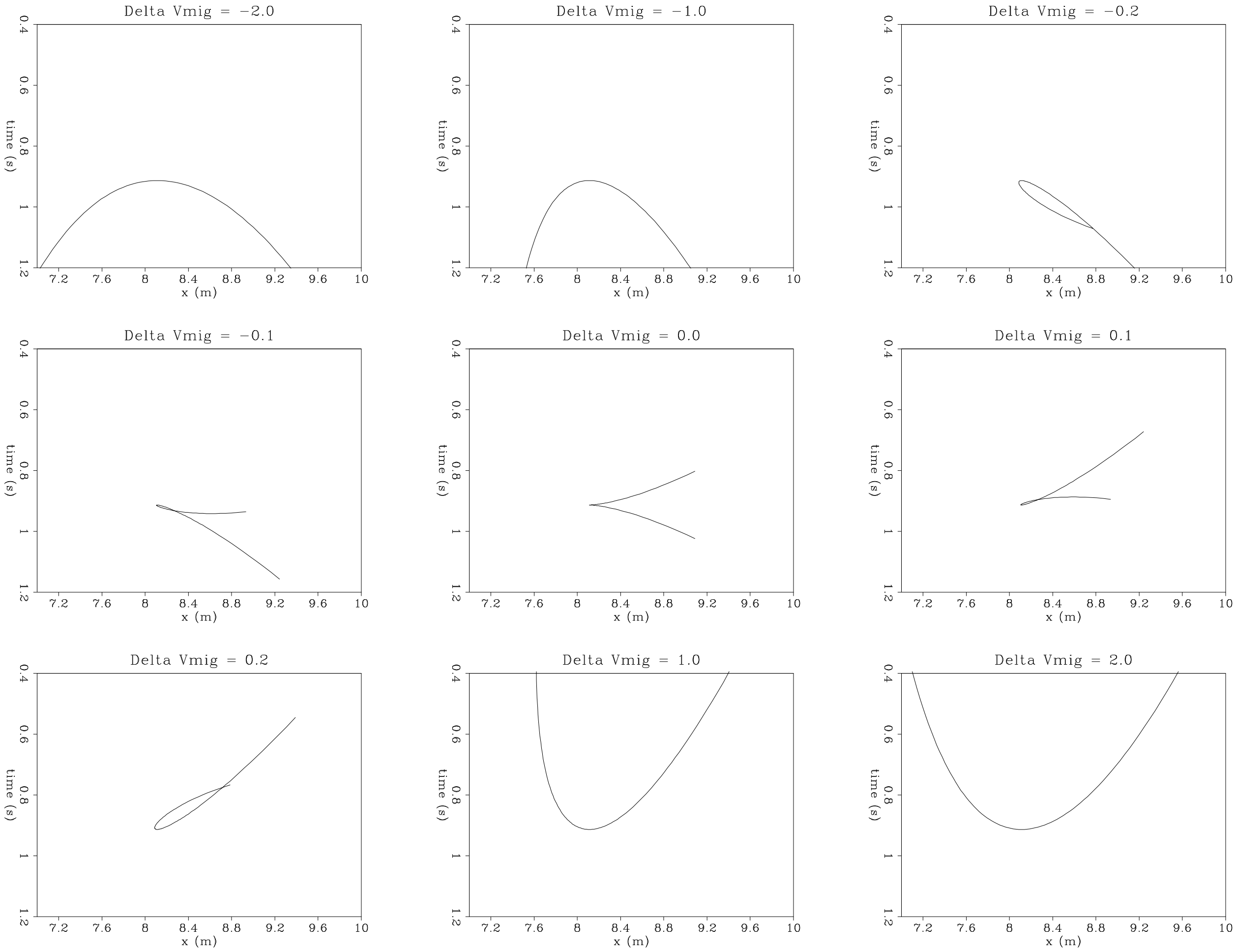

Figure 7: First-order theory of plume velocity dependence. The same migration velocities used in Figures 4 and 5 are used here. The center frame `Delta Vmig = 0.0` is generated using the RMS well velocity of 8.84 kft/s. It is the same curve that is overlaid on Figure 2. dimitri2-theory [ER]

The theoretical curves given by equations (13) and (14) are plotted in Figure 7 for the same values of migration velocity that are used in Figures 4 and 5. Notice that if $\triangle V_{mig} = 0$ equations (13) and (14) reduce to equations (1) and (2). The center frame of Figure 7 ($\triangle V_{mig} = 0$) is generated using the RMS well velocity. It is the same as the first-order curve overlaid on the migration result in Figure 2.

The first-order theory does not match the tangent construction (Figure 5) and Kirchhoff migration (Figure 4) results exactly; however, we can qualitatively follow the plume formation in Figure 7 just as we did in the other two cases. The curve progresses from an undermigrated frown to an overmigrated smile as the migration velocity increases. It is evident how the left limb of the frown curls around to form the upper limb of the plume ($\triangle V_{mig} = 0$) and later, as velocity increases even more, into the right side of the smile. Similarly, the right limb of the frown becomes the lower limb of the plume, and as velocity increases, it becomes the left side of the smile. We do not observe the slight clockwise rotation in the three middle frames with this simple first-order theory.

CONCLUSION

The response of time migration to a point diffractor in a `v(x)` medium is a cusp-shaped curve called a plume. Migration velocity analysis is strongly influenced by the behavior of the plume as the migration velocity is changed. We have examined the dependence of the zero-offset plume on migration velocity by migrating synthetic data. The observed velocity dependence is confirmed by the common-tangent construction. A simple first-order theory qualitatively explains the behavior of zero-offset time migration. It is clear that a more complete understanding of migration velocity analysis with time migration in a `v(x)` medium requires a finite-offset theory.

REFERENCES

Black, J. L., and Brzostowski, M. A., 1993, Systematics of time–migration errors: Accepted for publication in Geophysics.

Black, J. L., Bevc, D., Brzostowski, M. A., Mo, L.-W., and Palacharla, G., 1992, Plumes: Response of time migration to lateral velocity variation: SEP–**75**, 21–36.